Stator-flux-oriented Control of PMSM with highly-dynamic field-weakening operation

Martin Oettmeier, Carsten Heising, Volker Staudt and Andreas Steimel
Ruhr-University Bochum
D-44780 Bochum
Germany
Tel.: +49 234 32 23890
Fax.: +49 234 32 14597
Email: oettmeier@eele.rub.de, heising@eele.rub.de, staudt@eele.rub.de, steimel@eele.rub.de

***Abstract*—Excellent torque dynamics are important in traction applications – not because of acceleration or deceleration, but to meet additional demands as supression of drive chain oscillations, slip-slide protection and electronic stability control. Dynamics are limited by the rating and the switching frequency of the inverter, which the control has to make optimal use of. This paper presents a stator-flux-based control scheme for PMSM which gives the maximum physically possible dynamics with regard to the limitations stated above. The simulation results presented are based on a simulation structure which is verified by measurement and simulation carried out at an AFE.**

I. Introduction

The performance of magnet materials for permanent-magnet synchronous machines (PMSM) increases steadily [1]. By now, field strenght, field weakening and sensitivity to temperature no longer present problems. Decreasing cost promise affordable motors in the near future. With this background, PMSM become more and more important for practical use in light-rail, high-speed train and electric vehicle applications. The mass of the vehicles which adds to the effective inertia of motor and drive train, makes torque dynamics unimportant for acceleration and deceleration. However, high torque dynamics can be reached with electromagnetic motors and they are important – for suppressing disturbant oscillations and adding additional features to the vehicle performance, as slip-slide control and electronic stability control. In principle, dynamics are not limited at all – given unlimited control reserve. However, control reserve is never unlimited. In case of power-electronic converters size, weight and cost limit the available control quantity, given by the rating and the switching frequency of the converter. In order to keep the converter small, lightweight and cost-effective (and nevertheless with high efficiency), the control has to make optimal use of these limited resources.

This paper presents a stator-flux-based control scheme for PMSM. It bases on the Indirect Stator-quantities Control (ISC) scheme for asynchronous machines [2], [3], which is known for optimal performance also in the field-weakening range. Consequently, the control scheme presented gives the maximum physically possible dynamics with regard to the limitations stated above. The control scheme has also been the basis for the virtual-flux-based control of active front end converters (AFE) [4], [5]. The test bench for PMSM machines in our laboratory is not yet operational. Therefore, the simulation results presented are based on a simulation structure which is verified by previous measurement and simulation carried out at an AFE.

The control concept bases on the fundamental structure of a magnetic field in a rotating-field electromagnetic machine. A visualization of stator flux and rotor flux gives a graphic understanding of torque generation, which is in turn used to calculate the stator flux needed in the next step. For exact torque calculation, however, the co-energy method is used [6]. Torque calculation also takes into account the usual difference between the d-axis and q-axis inductances [7] – which is also not included in the graphic approach used to make the general methodology understandable.

II. Control concept of the PMSM

The main target of a machine control is to achieve the desired torque set-point value demanded by the application or the user. In addition the settling time is important in many applications. The control concept presented in this section gives a very fast transient behaviour by adjusting the output voltage of the machine inverter at changes of the desired torque as fast as phyically possible to its new values. The limitation remaining is mainly given by the rating (DC-link voltage and inductivity) and the switching frequency of the inverter used.

The priniciple used is similar to the Indirect Stator-Quantities Control (ISC) already known for asynchronous machines. The main difference is the air-gap rotor flux: In case of the ISC for asynchronous machines, the air-gap rotor flux results from the air-gap stator flux and rotor currents, induced by the relative rotation of the rotor with respect to the air-gap stator flux. In contrast the air-gap rotor flux of the permanent-magnet synchronous machine (PMSM) is defined by the rotor permanent magnets.

The principle of flux dispersion of all electromagnetic machines with rotating magnetic field can be displayed based on the example of an asynchronous machine (cp. fig. 1). This physical similarity gives the basis for a common control principle for such machines. The difference between the air-gap flux of the rotor $\Psi_{\delta,rotor}$ and the air-gap flux of the

978-1-4244-8218-4/10/$26.00 ©2010 IEEE

stator $\Psi_{\delta,stator}$ defines the actual torque as well as the field weakening of the machine. In the special case of a PMSM the direction of the main component of the rotor flux is equal to the actual orientation angle of the rotor.

The idea of the flux-based control of the PMSM is to directly compute the necessary stator flux of the machine to realise the desired torque and (if needed) the field weakening.

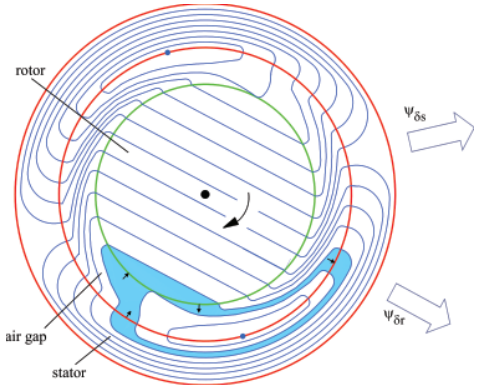

Fig. 1. example flux dispersion of electromagnetic machines with rotating magnetic field, here asynchronous machine

The difficulty of this approach is to obtain the desired air-gap flux of the stator which has to be set by the machine inverter. Mainly, the air-gap flux of the stator and the air-gap flux of the rotor are linked by the flux $\underrightarrow{\Psi}_{ag}$ which represents the elongation of the magnetic field in the air gap compared to the no-torque situation

$$\underrightarrow{\Psi}_{\delta,stator} = \underrightarrow{\Psi}_{\delta,rotor} + \underrightarrow{\Psi}_{ag}$$

. In case of the PMSM the main component of the air-gap rotor flux can be directly identified by the permanent flux Ψ_{PM} of the machine combined with the actual orientation angle χ.

$$\underrightarrow{\Psi}_{\delta,rotor} = \Psi_{PM} \cdot e^{j\cdot\chi}$$

In case of the PMSM, torque generation is a little more complex then stated here. A suitable basis for torque calculation is the co-energy [6], applied in the following two equations. The following application of these equations also neglects possible differences between d-axis and q-axis inductances, as they occur in case of interior-magnet PMSM. However, the control scheme described remains valid in such more complicated cases. The calculation of the desired stator flux needs slight modification in such a case.

$$P_{mech} = \omega \cdot \frac{3}{2} p |\Psi_{PM}| (-i_{s,\beta,des} \cos(\chi p) + i_{s,\alpha,des} \sin(\chi p)) \tag{1}$$

$$Q_{field} = \frac{3}{2} p |\Psi_{PM}| (i_{s,\alpha,des} \cos(\chi p) + i_{s,\beta,des} \sin(\chi p)) \tag{2}$$

Solving these equations with respect to the stator currents $i_{s,\alpha}$ and $i_{s,\beta}$ leads in combination with the main inductance of the machine to the air gap flux $\Psi_{ag} = L_{s,main} \cdot \underrightarrow{i}_s$.

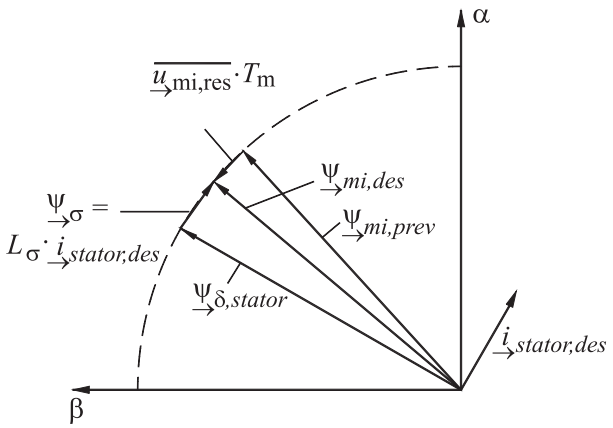

Fig. 2. Flux-based converter current control (generator operation mode)

The air-gap stator flux which has to be provided by the converter is

$$\underrightarrow{\Psi}_{\delta,stator} = \underrightarrow{\Psi}_{\delta,rotor} + \underrightarrow{\Psi}_{ag}$$

This flux can be realised by a standard flux-based control (cp. subsection II-A).

A. Flux-based subordinated control

To that purpose the actual flux $\underrightarrow{\Psi}_{\delta,stator}$ is computed. Processing the desired stator-current $\underrightarrow{i}_{s,des}$ as the pertaining leakage-flux space vector $\underrightarrow{\Psi}_{\sigma,des}$, the desired 'converter-flux' space vector of the motor inverter $\underrightarrow{\Psi}_{mi,des}$ is derived (Fig. 2, [4], [8]).

Using the information about the converter-flux space vector value $\underrightarrow{\Psi}_{mi,prev}$ of the previous sampling period, the resultant inverter-voltage space-vector reference value can be computed with:

$$\underrightarrow{u}_{mi,res} = \frac{d}{dt}(\underrightarrow{\Psi}_{mi,des} - \underrightarrow{\Psi}_{mi,prev}) \tag{3}$$

Discretisation of this equation leads to

$$\underrightarrow{\bar{u}}_{mi,res} = \frac{1}{T_m}(\underrightarrow{\Psi}_{mi,des} - \underrightarrow{\Psi}_{mi,prev}) \tag{4}$$

with the modulation period T_m (equal to the controller cycle time).

Finally the desired space vector of the output voltage is converted into phase notation under superposition of the necessary zero-sequence system and transferred to the PWM output of the control. The resulting switching functions are finally send via optical waveguides to gate units of the motor inverter.

B. Field weakening of the PMSM

Operating the PMSM in high-speed mode above rated speed requires the PMSM control to master field weakening. Describing this mode in a demonstrative way, the motor inverter – limited by its DC-link voltage – is not able to maintain the rotation speed of the stator-flux linkage $\Psi_{\delta,stator}$. To be able to further increase the speed, the amplitude of the stator-flux

linkage has to be adapted to the available DC-link voltage. In contrast to state-of-the-art field-oriented control, no extensions are necessary in case of stator-flux-oriented control. Only set-point values have to be chosen suitably for the desired working points. In almost every application this means a reduction of the stator-flux linkage. In the simulation section (cp. section IV) field weakening is presented.

III. Comparison of Simulation and Measurement Results for an Active Front End

Because a PMSM with an appropriate motor inverter was not yet at hand to verify the derived PMSM control, a simulation was employed. In this section the correct emulation of an Active Front End – identical with a motor inverter and with similar control scheme – is verified by a comparison of simulation result and measurement.

The three-phase side of the converter is connected to the 50-Hz lab grid by three inductances $L_\sigma = 250\,\mu\text{H}$. Thereby the line-to-line voltage of the grid has a peak voltage of 540 V reduced from the nominal voltage of $\hat{u}_{12\text{N}} = \sqrt{2}{\cdot}400\,\text{V} = 566\,\text{V}$ by the winding ratio $\frac{w_p}{w_s} = 1.048$ of the used transformer. On the converter DC side a resistor was connected in parallel to the DC-link via a switch causing a step load current of 150 A, yielding an active power of 90 kW. The phase currents are counted positively out of the converter.

Figure 3 shows the measured transient response of the Active Front End. The transient time of three periods is due to the robust control parameters chosen for commissioning. An advantage of these parameters is the well-damped transient response with marginal overshoot of the DC-link voltage. In the same manner the AC currents offer a well-damped transient behaviour leading to steady-state amplitude and (nearly) sinusoidal waveform within only two half periods.

The optimal 30°-phase shift between measured line-to-line voltage and negative line current can be clearly idendentified. Thus, the proper operation of the chosen control is proven by the transient response upon a 90-kW load step.

In order to verify the used simulation approach, the real parameters of the test bench have been used in combination with the set of first-order differential equations [9], the same control algorithm and the same load step (Fig. 4). Besides the mentioned peak-to-peak voltage of $\hat{u}_{pg} = 566\,\text{V}$ and the coupling inductance of $L_{\sigma pg} = 250\,\mu\text{H}$, a parasitic resistance of $R_{pg} = 1\,\text{m}\Omega$ is assumed, the winding ratio of $\frac{w_p}{w_s} = 1.048$ is neglected. The parameters of the DC-link components are as follows: a DC-link capacitor of $C_{DC} = 4.2\,\text{mF}$ and its parallel parasitic resistance of $R_{DC} = 12\,\text{k}\Omega$.

It can be clearly seen that simulation and measurement results fit very good. The voltage drops of the DC-link capacitor equal and the resulting transient response times forced by the used controller have the same size. In the same manner the only differences between amplitude, phase angle and shape of the simulated and the measured currents are noise and peaks caused by the measurement hardware. Based on this perfect match verifying the high accuracy of the chosen simulation

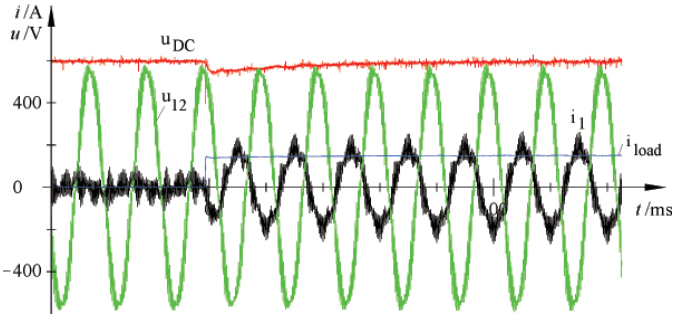

Fig. 3. Measurement results of Active Front End with 90 kW load step at $t = 0\,\text{s}$

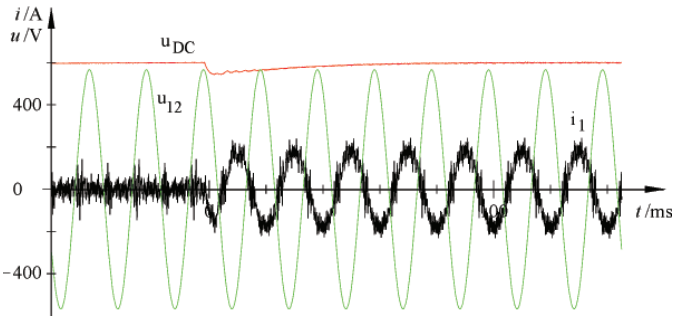

Fig. 4. Simulation results of Active Front End with 90 kW load step at $t = 0\,\text{s}$

approach, the forthcoming analysis of the control performance is done using the simulation.

IV. Simulation Results of the PMSM Control

Having verified the simulation of a motor inverter verified (cp. III) and with an appropriate model of the PMSM, the control concept derived (cp. section II) can be verified.

In this scenario the sampling time of the motor inverter is set to 125 μs, the DC-link voltage equals 600 V. The switching frequency is 4 kHz. The angular frequency of the rotor is at $\omega_r = 2 \cdot \pi \cdot 150\,\text{Hz}$. To emulate a typical laboratory set up – the machine under test is mechanically coupled with a speed-controlled separately excited DC machine to test the torque control in a safe environment – here the inertia of the modelled PMSM is set to a very high value, thus leading to the constant rotation speed of ω_r.

The PMSM emulated in this simulation has a stator main inductance of $L_m = 90\,\mu\text{H}$, a leakage inductance of $L_\sigma = 10\,\mu\text{H}$ and a parasitic resistance of $R_\sigma = 38.3\,\text{m}\Omega$ ($L_d = L_q = 100\,\mu\text{H}$). The flux of the permanent magnet is set to a rms value of $\Psi_{PM} = 37\,\text{mVs}$ (EV machine for 216-V battery voltage).

In the following simulation results a test run of the PMSM flux-based control is presented. In detail the torque control is checked by maintaining a constant rotation speed. Here the torque set points are varied abruptly, analysing the resulting torque at the machine.

Figure 5 shows an overview of the performed test scenario. From $t_1 = 310\,\text{ms}$ the torque set point is 0 Nm. The first torque step is performed at $t_2 = 320\,\text{ms}$ ($-12\,\text{Nm}$). In the

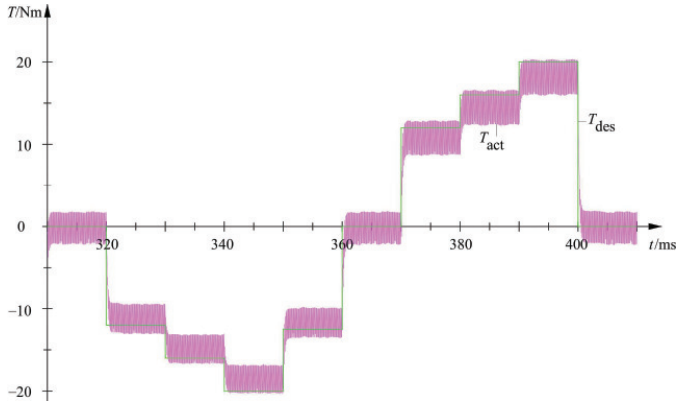

Fig. 5. Torque overview

following the torque is varied to $-16\,\mathrm{Nm}$ ($t_3 = 330\,\mathrm{ms}$), $-20\,\mathrm{Nm}$ ($t_4 = 340\,\mathrm{ms}$), $-12.5\,\mathrm{Nm}$ ($t_5 = 350\,\mathrm{ms}$) back to $0\,\mathrm{Nm}$ ($t_6 = 360\,\mathrm{ms}$). The same iteration is done for positive torque set points, ending the test with a high torque-step from $20\,\mathrm{Nm}$ to $0\,\mathrm{Nm}$ at $t_{10} = 400\,\mathrm{ms}$. It can be cleary seen that the desired torque T_{des} satisfactory equals the actual torque T_{act} with only a few percent difference. This difference is due to the fact that the flux-oriented control implemented here has no additional integral part in the control structure, thus allowing small differences between actual and desired torque.

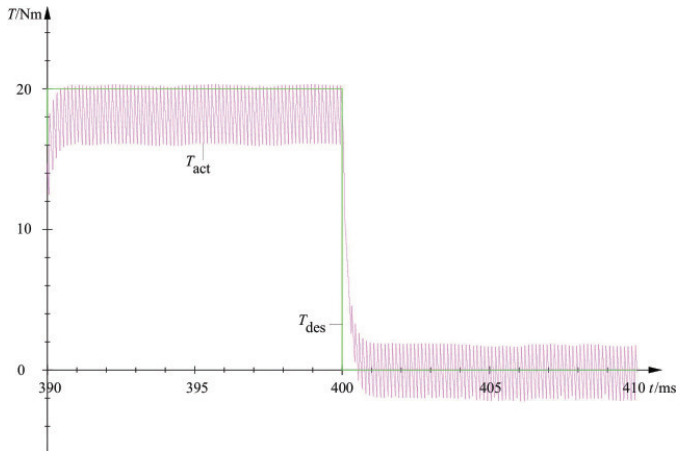

Fig. 6. Zoom of torque set-point change at $t_9 = 390\,\mathrm{ms}$ ($16\,\mathrm{Nm}$ to $20\,\mathrm{Nm}$) and $t_{10} = 400\,\mathrm{ms}$ ($20\,\mathrm{Nm}$ to $0\,\mathrm{Nm}$)

Figure 6 includes a zoom of the last two torque load steps performed before (cp. fig. 5). It can be observed that the steady-state operation is obtained within $1\,\mathrm{ms}$ after the load step.

Figure 7 shows the stator currents, pertaining to the torque waveform displayed. In addition the stator current in q-direction is displayed. This quantity is especially computed for demonstration issues, it is not used in the computation algorithms of the control. The rotational frequency of the rotor ($f_r = 150\,\mathrm{Hz}$) can be cleary identified. During the 20-Nm set point the amplitude of the stator currents is about $\hat{i}_s = 237\,\mathrm{A}$. Having the amplitude of the machine-inverter output-voltage

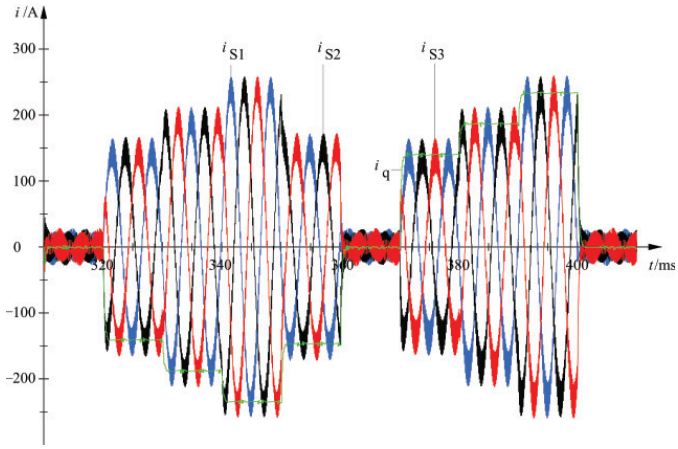

Fig. 7. Stator currents upon torque load-steps

close to the voltage induced by the rotor $\hat{u}_i = \omega \cdot \hat{\Psi}_{PM}$ an active power of $P_{el} = 3 \cdot \frac{\hat{u}_i \cdot \hat{i}_s}{2} = 17.5\,\mathrm{kW}$ can be computed.

The demonstrated simulations of the PMSM control show proper service in all operation modes.

In the following, the impact of field-weakening dynamics is analysed. For this purpose, the set-point value of the torque is set to zero, the PMSM is driven by a speed-controlled separately excited DC machine. Thus, a stator current close to zero is expected. Figure 8 shows field weakening for a PMSM with a permanent flux $\Psi_{PM} = 48\,\mathrm{mVs}$ and a main inductance of $200\,\mathrm{mH}$. At $t = 0.358\,\mathrm{s}$ field control is activated, leading first to an increase of the stator flux. At $t = 0.408\,\mathrm{s}$, the set-point of the field-weakening control is reversed, reducing the stator flux. At $t = 0.458\,\mathrm{s}$, field weakening is turned off. In the figure the stator current of the first leg is displayed. In addition, the output voltage of the motor inverter is illustrated. In contrast to the switched output voltage, the symmetrized desired voltage of the PWM is shown. Only reactive power is transferred from the motor inverter, apparent at the $90°$ phase shift of voltage and current. The desired value of the torque is zero, thus, the pictured torque value is close to zero.

Figure 9 shows the space-vector (s.v.) trajectory of the virtual-flux of the motor inverter which – together with the leakage flux – leads to the stator flux of the PMSM. Figure 9 does not include any information of time due to the parametric presentation in $\alpha - \beta$-coordinates. The outer circle shows the flux s.v. during the interval $t \in [0.358;\ 0.408]$. Here, it can be cleary seen that the flux is boosted in comparison to the flux in idle mode (central circle). Flux weakening can be identified in the interval $t = [0.408;\ 0.458]$ to which the small circle is associated.

V. Conclusion

In this paper, a flux-based control of a permanent-magnet synchronous machine (PMSM) is presented. Possible applications include light railways and electric vehicles. The control scheme is based on the Indirect Stator-quantities Control (ISC) known for induction machines and similar for virtual-flux-based control schemes for active front ends (AFE). It

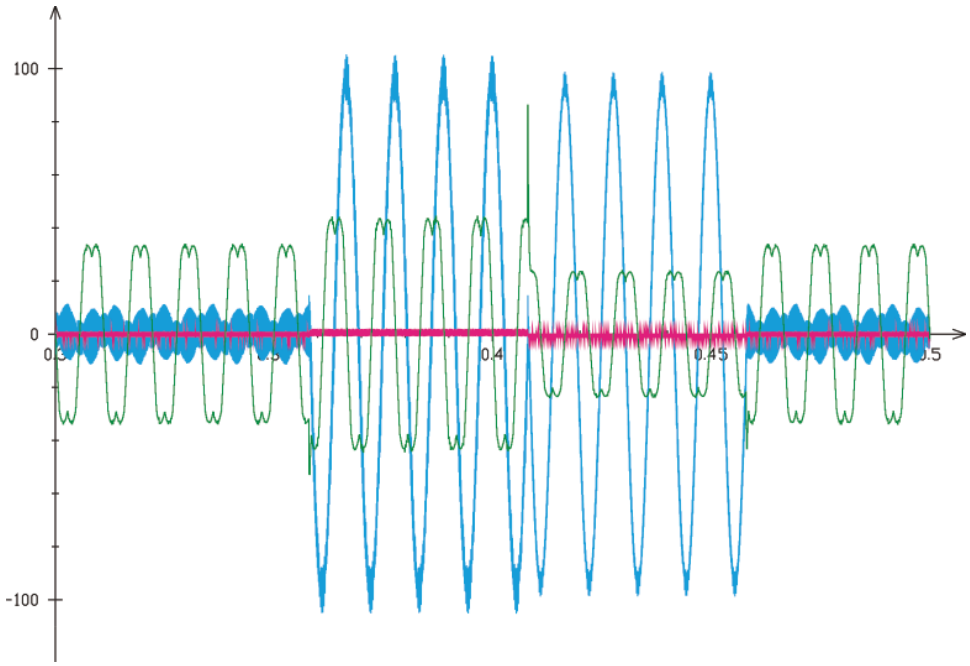

Fig. 8. Amplification and weakening of main flux of PMSM, no load operation, $f_s = 90\,\text{Hz}$; red: torque ($= 0$), blue: stator current i_{sa}, green: stator voltage

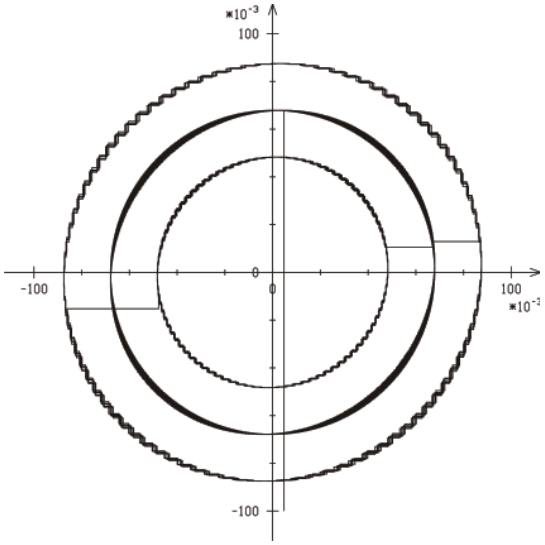

Fig. 9. Field weakening – desired space vector trajectory of the machine-inverter virtual flux

offers excellent torque dynamics, utilizing rating and switching frequency of the converter in an optimal way. Excellent torque dynamics give a solid basis for added drive features like slip-slide protection or electronic stability control even in field-weakening operation. The properties of the control are demonstrated based on simulation. The simulation concept has been verified by comparing measurement and simulation for an AFE, because a PMSM test bench is not yet available.

ACKNOWLEDGEMENTS

This work has been performed with support of the Karl-Vossloh-Stiftung, Germany. The opinions expressed by the authors do not necessarily reflect the position of the Karl-Vossloh-Stiftung, nor does the work involve any responsibility on its part.

REFERENCES

[1] G. Liew, N. Ertugrul, W. L. Soong, and J. Gayler, "An investigation of advanced magnetic materials for axial field brushless permanent magnet motor drives for automotive applications," in *Power Electronics Specialists Conference (PESC)*, (Jeju, Korea), 2006.

[2] A. Steimel, *Electric Traction - Motive Power and Energy Supply*. Muenchen: Oldenbourg Industrieverlag, 2008.

[3] M. Jnecke and F. Hoffmann, "Fast torque control of an igbt-inverter-fed three-phase a.c. drive in the whole speed range - experimental results," in *6th Europ. Conf. on Power Electronics, Vol. 3*, (Sevilla), pp. 399–404, 1995.

[4] M. Weinhold, "A new control scheme for optimal operation of a three-phase voltage dc link pwm converter," in *PCIM 91 - International Intelligent Motion Conference*, 1991.

[5] M. Malinowski, M. Kazmierkowski, S. Hansen, F. Blaabjerg, and G. Marques, "Virtual-flux-based on direct power control of three-phase pwm rectifiers," *Industry Applications, IEEE Transactions*, vol. 37, Issue 4, pp. 1019–1027, Jul/Aug 2001.

[6] A. E. Fitzgerald, C. Kingsley, and S. D. Umans, *Electric Machinery*. New York: McGraw-Hil, 2003.

[7] S. Morimoto, Y. Takeda, T. Hirasa, and K. Taniguchi, "Expansion of operating limits for permanent magnet motor by current vector control considering inverter capacity," *IEEE Transactions on Industry Applications*, vol. 26, pp. 866–871, 1986.

[8] M. Malinowski, M. Kazmierkowski, S. Hansen, F. Blaabjerg, and G. Marques, "Virtual-flux-based direct power control of three-phase pwm rectifiers," *IEEE Transaction son Industry Applications*, 2001.

[9] C. Heising, R. Bartelt, V. Staudt, and A. Steimel, "Single-phase 50-kw, 16.7-hz four-quadrant line-side converter for railway traction applications," in *13th International Power Electronics and Motion Conference*, (Poznan, Polen), 2008.